

# Utilization of $\text{TiO}_2/\text{gC}_3\text{N}_4$ nanoadditive to boost oxidative properties of vegetable oil for tribological application

Nisha RANJAN<sup>1,2</sup>, Rashmi C. SHENDE<sup>1</sup>, Muthusamy KAMARAJ<sup>2</sup>, Sundara RAMAPRABHU<sup>1,\*</sup>

<sup>1</sup> Department of Physics, Indian Institute of Technology Madras, Chennai 600036, India

<sup>2</sup> Department of Metallurgical and Materials Engineering, Indian Institute of Technology Madras, Chennai 600036, India

Received: 04 June 2019 / Revised: 10 September 2019 / Accepted: 17 October 2019

© The author(s) 2019.

**Abstract:** The emergence of vegetable oil as a promising alternative lubricant in the tribological application space has fueled research for making these oils as useful as mineral oils. Tribological modification of vegetable oil by the addition of  $\text{TiO}_2/\text{gC}_3\text{N}_4$  nanocomposite (as a nanoadditive) was studied here. The dispersion of the nanoadditive in the vegetable oil showed good oil dispersion stability without the addition of any surfactant. The tribological studies were conducted in a four-ball tester using ASTM standard D5183. In addition, the effect of temperature on tribological performance was also studied to understand the oxidation behavior of vegetable oil. The results showed a significant improvement in friction and wear properties of the optimized nano-oil. The mechanism behind the improvement in friction and wear properties is annotated in this paper.

**Keywords:**  $\text{TiO}_2/\text{gC}_3\text{N}_4$  nanoadditive; vegetable oil; oxidation

## 1 Introduction

In recent years, the use of vegetable oil has gained popularity due to the oil's renewability, inherent biodegradability, and low eco-toxicity [1–3]. This is indeed advantageous because mineral oil (a petroleum product) is non-renewable and toxic. Apart from these advantages, vegetable oil also has a superior flash point, better viscosity index, good lubricity, and better metal adherence [1]. Vegetable oils consist mostly of fatty acids, which can be in the form of saturated and unsaturated hydrocarbons. Reports suggest that the presence of polar groups with long hydrocarbon chains allows vegetable oil to possess better adhesion, which can greatly enhance the boundary layer lubrication performance [4]. In boundary layer lubrication, a thin protecting layer of lubricant (also termed “tribo-film”) gets adsorbed between the contact zone during the relative motion and provides a large decline in the coefficient of friction, wear properties, and accumulation of heat. The reason for

the large decline is basically because of the masking of force fields acting on the underlying surfaces [4]. Therefore, the interaction between the underlying surface and the lubricant plays a major role in improving the tribological performance. However, these oils have poor thermo-oxidative properties and may undergo changes in chemical and physical composition at elevated temperatures and pressures, which restricts their widespread use for tribological applications [2, 5–7]. To improve these properties, the molecular structure may be modified or additives may be added to the oils [8].

In our work, we chose  $\text{TiO}_2/\text{gC}_3\text{N}_4$  nanocomposite as an additive to modify the oil for better tribological performance. The main role of an additive is to improve the friction and wear performance of oils at high speed, temperature, and load [9–11]. Essentially, all lubricants contain additives to improve their inherent properties. Syahrullail et al. noted that vegetable oil has the potential to replace mineral oil if a proper selection of additive is done [6]. There are a

\* Corresponding author: Sundara RAMAPRABHU, E-mail: ramp@iitm.ac.in

number of additives that can improve the tribological performance of the base oil, either mineral oil or vegetable oil. At this point, the selection of additives becomes an important step to solve certain problems such as friction, wear, extreme pressure, oxidation, dispersion, etc. Some common additives such as graphite, molybdenum disulfide ( $\text{MoS}_2$ ), hexagonal boron nitride (h-BN), and zinc dialkyldithiophosphates (ZDDP) are used for antiwear, extreme pressure, and corrosion resistance applications [12–14]. However, at elevated temperatures, elements such as sulfur, phosphorus, carbon, and nitrogen convert into oxides, creating a toxic environment and leading to the formation of ash, which blocks machine filters. This reduces the life of engine components [14, 15]. Therefore, there is a large demand for environmentally friendly lubricants with lower additive contents. As an alternative, nanomaterials have been explored extensively for tribological applications because of their special properties, such as large surface to volume ratio with smaller size, which make them suitable for rolling, polishing, mending effects, and uniform tribofilm formation [16, 17]. Some well-known metal oxide nanoparticles such as  $\text{ZrO}_2$ ,  $\text{TiO}_2$ ,  $\text{Fe}_3\text{O}_4$ ,  $\text{Al}_2\text{O}_3$ ,  $\text{CuO}$ , and  $\text{ZnO}$ , which provide excellent antiwear properties, have been used widely as additives for the improvement of the tribological performance of lubricants [18–22]. Similarly, some common layered nanomaterials such as graphene,  $\text{WS}_2$ ,  $\text{MoS}_2$ , and h-BN have been explored [18]. Moreover, uniform tribofilm formation has been found in structures like graphene, nitrogen-doped graphene,  $\text{MoS}_2$  [23], and diamond-like carbon films, which result in a huge reduction in friction and wear because of the pushed sliding motion between the interlayers [17, 24, 25]. Graphitic carbon nitride ( $\text{gC}_3\text{N}_4$ ) is another layered nanomaterial having a graphene-like structure [26]. This material is porous, hard, chemically inert, and biocompatible [27]. Its superior lubricating properties have been reported in the literature [28–31]. However, the dispersion of  $\text{gC}_3\text{N}_4$  in media may require surface modification or functionalization. Yang et al. showed an enhancement in tribological performance by surface modification of  $\text{gC}_3\text{N}_4$  with copper nanoparticles [32]. Later, Kumar et al. reported on octadecylamine grafted  $\text{gC}_3\text{N}_4$ , which showed a 44% reduction in the coefficient of friction value [33]. In view of the above, it can be ascertained

that the tribological properties of  $\text{gC}_3\text{N}_4$  can be enhanced either by obtaining hybrids with metal or metal oxide nanoparticles or by chemical modification of  $\text{gC}_3\text{N}_4$  sheets [30, 34–36].

Here, we utilized  $\text{TiO}_2$  nanoparticles to stabilize the dispersion and harvest the tribological properties it offers. It has been well documented in the literature that  $\text{TiO}_2$  (anatase) nanoparticles show excellent stability in lubricant oils but a slight reduction in the coefficient of friction and wear properties. These nanoparticles aid the formation of film between surfaces [37]. Apart from its stability and tribological properties, it should also be noted that  $\text{TiO}_2$  is an easily accessible metal oxide that is non-toxic and safe for the environment [38, 39]. In this work, we prepared  $\text{TiO}_2/\text{gC}_3\text{N}_4$  nanocomposite via a combination of sol gel for  $\text{TiO}_2$  synthesis and solid-state reaction for the nanocomposite. The tribological property enhancement caused by the dispersion of the  $\text{TiO}_2/\text{gC}_3\text{N}_4$  in vegetable oil was investigated using a four-ball tester.

## 2 Experimental section

### 2.1 Materials

For  $\text{TiO}_2$  synthesis, titanium (IV) isopropoxide (TTIP) (Spectrochem, 98% purity), acetic acid (Sigma Aldrich), and sodium hydroxide (Merck, 97% purity) precursors were used. Millipore distilled water was used as a reagent.  $\text{gC}_3\text{N}_4$  was prepared by using urea (Merck, 99.5% purity) as a precursor.

### 2.2 $\text{TiO}_2$ synthesis

$\text{TiO}_2$  nanoparticles were prepared in the laboratory using an acid-assisted sol-gel route [40]. TTIP was mixed in distilled water in the ratio of 1:10 and the mixture was stirred vigorously. This was followed by addition of acetic acid and heating at 80 °C for 5 h. After cooling, 10 ml of 2 M sodium hydroxide was added to make the solution basic. Then, the white precipitate obtained was washed, filtered, dried at 120 °C, and used for nanocomposite synthesis.

### 2.3 $\text{gC}_3\text{N}_4$ synthesis

The formation of  $\text{gC}_3\text{N}_4$  from urea has been reported widely in the literature [41–44]. For comparison with

TiO<sub>2</sub>/g-C<sub>3</sub>N<sub>4</sub> nanoadditive, gC<sub>3</sub>N<sub>4</sub> synthesis was also done from urea. In this process, urea was taken in an alumina crucible and pyrolyzed in a muffle furnace at 550 °C for 2 h with a heating rate of 10 °C.

#### 2.4 TiO<sub>2</sub>/gC<sub>3</sub>N<sub>4</sub> synthesis

The as-prepared TiO<sub>2</sub> nanoparticles were utilized in the subsequent step of synthesis by mixing them with urea and then annealing to prepare TiO<sub>2</sub>/gC<sub>3</sub>N<sub>4</sub>. To obtain the TiO<sub>2</sub>/gC<sub>3</sub>N<sub>4</sub> nanocomposite, the uniform mixture of urea and as-prepared TiO<sub>2</sub> was then heated at 550 °C for 2 h in a continuous argon flow in a tubular furnace with a heating rate of 10 °C.

#### 2.5 Nano-oil preparation

The TiO<sub>2</sub>/gC<sub>3</sub>N<sub>4</sub> nanocomposite was dispersed in vegetable oil (groundnut oil) to prepare nano-oil of various concentrations: 0.00625 mg/ml, 0.0125 mg/ml, 0.0187 mg/ml, and 0.025 mg/ml. The base oil consisted of both saturated and unsaturated fatty acids. It had an unsaturated/saturated fatty acid ratio of 4. Two saturated fatty acids, palmitic acid and stearic acid, were present in the composition. The unsaturated fatty acids present were oleic acid and linolenic acid. The dispersion was carried out by using a probe sonicator (Sonics, 500 W) for 30 min with a frequency of 20 kHz, power of 500 W, and amplitude of 20%. The stability of the prepared nano-oil was analyzed by UV–Vis spectroscopy (Cary 100 UV Visible, Agilent Technologies) and a sedimentation method. All concentrations of this nano-oil were then used to evaluate the coefficient of friction (COF) and wear property of the oils.

#### 2.6 Characterization

The obtained TiO<sub>2</sub>/gC<sub>3</sub>N<sub>4</sub> nanocomposite was characterized using a Rigaku X-ray diffractometer with Cu K<sub>α</sub> radiation ( $\lambda = 0.154$  nm and  $10^\circ \leq 2\theta \leq 80^\circ$ ). Scanning electron microscopy (SEM) with energy dispersive spectroscopy (EDS) (Quanta 400, FEI) was used for structural and qualitative compositional analysis. Transmission electron microscopy (TEM) imaging (CM12, Philips, 200 kV) was performed on the samples to investigate the structural features of the nanoparticles at higher resolution. The thermal

decomposition properties of the nanocomposite were analyzed by thermogravimetric analyzer (TGA) (SDTQ600, TA Instruments) from room temperature (RT) to 1,000 °C at a heating rate of 10 °C/min. Furthermore, the thermal degradation of the base oil was also evaluated using TGA analysis at the temperature range of 25 to 200 °C. The measurements were performed with a heating rate of 5 °C/min and flow rate of air of 100 μl/min. Attenuated total reflectance–infra-red (ATR–IR) analysis of the base oil was carried out using an Agilent Cary 630 diamond ATR by placing the powder sample directly on the diamond crystal.

The tribological properties were studied by using a four-ball tester (Magnum Engineers, Bengaluru, India). The four-ball tester is an analytical tool that can measure the tribological performance of lubricants using a four-ball oil assembly. In the four-ball oil assembly, three stationary balls are kept in a holder, which contains oil (oil bath holder), and the fourth ball is attached to the top holder, which is in intimate point contact with the three stationary balls. It was rotated at 600 rpm with an applied load of 400 N, according to ASTM standard D5183. There is an in-built heater in the oil bath holder to maintain the temperature according to ASTM standards. The measurement provides the frictional torque, which can be converted to the COF. These data were obtained with the aid of a torque sensor attached to the oil bath holder. The tested samples were analyzed further by microscope for wear analysis. The test balls used for the testing were made of high carbon, high chromium (HCHC) alloy and had a diameter of 12.7 mm. These steel balls have high corrosion and wear resistance, according to ANSI standard. To investigate the temperature dependence of the nanoadditive efficiency, a lower operating temperature (room temperature) was chosen for the experiments. The other parameters were kept constant. The surface morphology of the worn area was analyzed by SEM imaging (Quanta 200) at an accelerating voltage of 15–30 keV. Wear scar surface roughness was also analyzed using a non-contact surface profiler (AEP Nanomap 1000 WLI). Viscosity measurements were performed using a Brookfield R/S rheometer. The shear rate used for the measurement was 1,000 s<sup>-1</sup>.

### 3 Results and discussion

#### 3.1 Structural, morphological, and thermal stability analyses

Powder X-ray diffraction (XRD) studies were carried out to determine the structural characteristics of  $gC_3N_4$ ,  $TiO_2$ , and  $TiO_2/gC_3N_4$ . The XRD data are displayed in Fig. 1. Annealing of urea at 550 °C yields  $gC_3N_4$ , and this can be confirmed by the peaks appearing at 13° and 27°, which correspond to the (100) and (002) diffraction planes for periodically stacked graphitic materials [30, 42]. The sol–gel synthesis of  $TiO_2$  yielded a nanocrystalline structure, the diffraction pattern, and the material was indexed to a single phase tetragonal  $TiO_2$  anatase (ICDD card No. 98-010-9333). Well-defined sharp peaks confirm the higher degree of crystallinity prevalent in the material. In the case of  $TiO_2/gC_3N_4$ , the diffraction pattern shows peaks corresponding to  $TiO_2$  anatase; however, no discernable  $gC_3N_4$  peak can be observed. This may be attributed to the high degree of crystallinity exhibited by  $TiO_2$ , which results in suppression of the low-intensity  $gC_3N_4$  peaks. Similar observations have been reported in the literature [30, 45]. The average crystallite size was estimated in accordance with the Scherrer formula ( $d = 0.9\lambda/B\cos\theta$ ), where  $d$  is crystallite size,  $\lambda$  is Cu- $\alpha$  radiation (0.15406 nm),  $B$  is full width half maxima, and  $\theta$  is the Bragg angle, calculated to be 20.22 and 20.94 nm for  $TiO_2$  and  $TiO_2/gC_3N_4$ , respectively.

Figure S1 in the Electronic Supplementary Material (ESM) shows SEM images of the  $TiO_2$ ,  $gC_3N_4$ , and

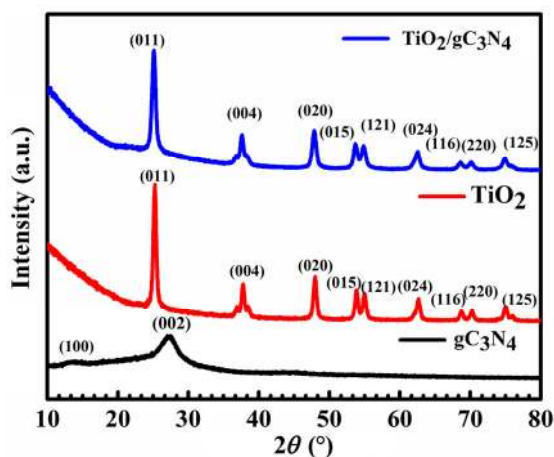


**Fig. 1** Powder XRD pattern of  $gC_3N_4$ ,  $TiO_2$ , and  $TiO_2/gC_3N_4$  nanocomposite.

$TiO_2/gC_3N_4$  and EDS data of the  $TiO_2/gC_3N_4$ . It can be observed that the  $TiO_2$  nanoparticles are very small, on the order of 30–40 nm. The  $gC_3N_4$  prepared from urea exhibits a porous sheet-like morphology. SEM images of the  $TiO_2/gC_3N_4$  nanocomposite show that the  $TiO_2$  decoration over the  $gC_3N_4$  sheets is uniform and even. It can be seen that the signals for titanium and oxygen are very strong, whereas those for nitrogen and carbon are weak. Because the EDS signal strength is proportional to the amount of element present, it may be inferred that the  $gC_3N_4$  content is lower than the amount of  $TiO_2$ . This observation is consistent with the XRD data, in which no discernable  $gC_3N_4$  peak was observed. To gain a deeper insight, TEM imaging of the  $TiO_2/gC_3N_4$  nanocomposite was carried out. As shown in Figs. 2(a) and 2(b), sheets surrounded by  $TiO_2$  nanoparticles are visible in the material at very high magnifications. Both images were taken at two different places in order to confirm the morphology throughout the sample. The  $gC_3N_4$  sheets tend to be folded, which explains their small size, and no prominent aggregation of  $TiO_2$  nanoparticles was observed.

To understand the thermal stability of the nanoadditive, TGA was performed on  $TiO_2$ ,  $gC_3N_4$ , and  $TiO_2/gC_3N_4$  nanoadditive from RT to 1,000 °C in an air atmosphere. Figure 2(c) shows the TGA curves for  $TiO_2$ ,  $gC_3N_4$ , and  $TiO_2/gC_3N_4$  nanoadditive. In only the case of  $TiO_2$  nanoparticles, the curve depicts no significant weight loss until 1,000 °C. However, for  $gC_3N_4$ , there is large decline at 550 °C due to the fact that the carbon and nitrogen oxidize in air and form carbon dioxide and other volatile gases. For the  $TiO_2/gC_3N_4$  nanoadditive, two thermal transitions can be observed. The first one shows a 1% weight loss from 30–100 °C, which corresponds to desorption of the water molecules. The second transition, observed in the range of 600–1,000 °C, shows a 4% weight loss, which can be attributed to the oxidation of the  $gC_3N_4$ . The total amount of weight loss observed in the composite is 5%. Therefore, it can be inferred from the curve that the total amount of  $gC_3N_4$  in the sample is relatively very small and that the prepared nanoadditive is very thermally stable to 500 °C. It should also be noted that an increase in operating temperature may cause degradation of the molecular structure of the vegetable oil, which leads to detachment of the

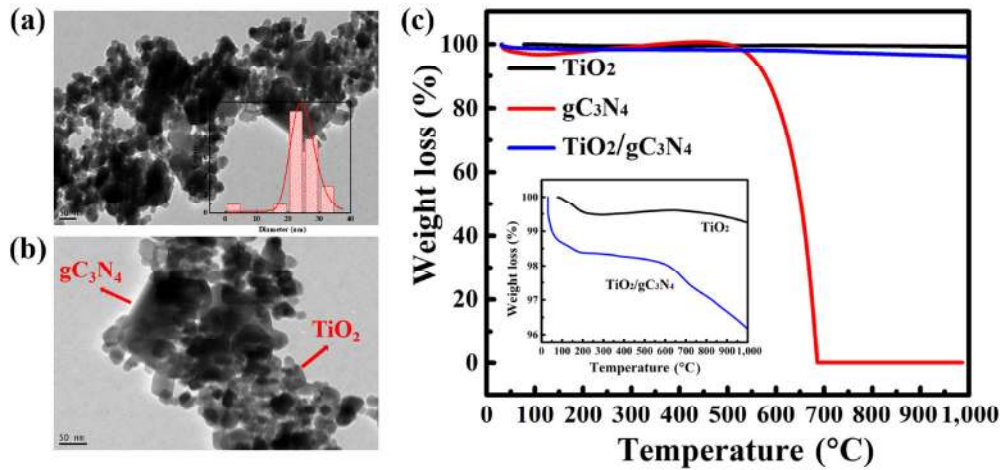


**Fig. 2** (a, b) TEM images of  $\text{TiO}_2/\text{gC}_3\text{N}_4$  nanoadditive, and (c) TGA curve of  $\text{TiO}_2$ ,  $\text{gC}_3\text{N}_4$ , and  $\text{TiO}_2/\text{gC}_3\text{N}_4$  nanoadditive.

tribo-film formed on the surface [46, 47]. However, the role of  $\text{TiO}_2/\text{gC}_3\text{N}_4$  during such high temperature applications seems promising.

### 3.2 Vegetable oil (base oil) properties

To understand the lubrication properties of vegetable oil, chemical analysis of the same is of utmost importance. As discussed earlier, the only drawback of vegetable oil is its poor oxidative performance. Figure 3(a) shows the IR spectrum of the base oil, which confirms the presence of both saturated and unsaturated bonds in the structure. The two intense peaks observed at  $2,921.5$  and  $2,852.5\text{ cm}^{-1}$  confirm the presence of asymmetric and symmetric vibrations of  $=\text{CH}_2$  bonds. A small peak observed at  $3,003\text{ cm}^{-1}$  is an indication of a high degree of unsaturation [48]. The peak observed at  $1,740\text{ cm}^{-1}$  is the common peak highlighting the saturated bonds present in fatty acids. The peaks observed between  $1,300$  and  $1,500\text{ cm}^{-1}$

correspond to the vibration of deformation  $\delta(\text{C-H})$ . The other peaks, as we move to lower wavenumbers, correspond to the common vibrations of  $\text{C=O}$  and  $\text{C=C}$ . Figure 3(b) shows the TGA–DTA curve of the base oil. It can be seen from the curve that the base oil shows only a 2% degradation until  $200\text{ }^\circ\text{C}$ . Although the onset temperature for decomposition is  $140\text{ }^\circ\text{C}$ , 100% decomposition of the base oil does not occur until  $600\text{ }^\circ\text{C}$ , as shown in Fig. S2 in the ESM. Degradation involves the breakdown of oxygenated hydrocarbons to lower molecular weight volatile hydrocarbons. It has been documented in the literature that the decomposition of saturated fatty acids is much faster than that of unsaturated fatty acids because they first undergo the uptake of oxygen to form hydroperoxides succeeded by ketone and aldehyde formation [49]. As shown in Fig. 3(b), there is no weight gain in the TGA curve, which indicates the presence of saturated fatty acids in a larger amount. However,

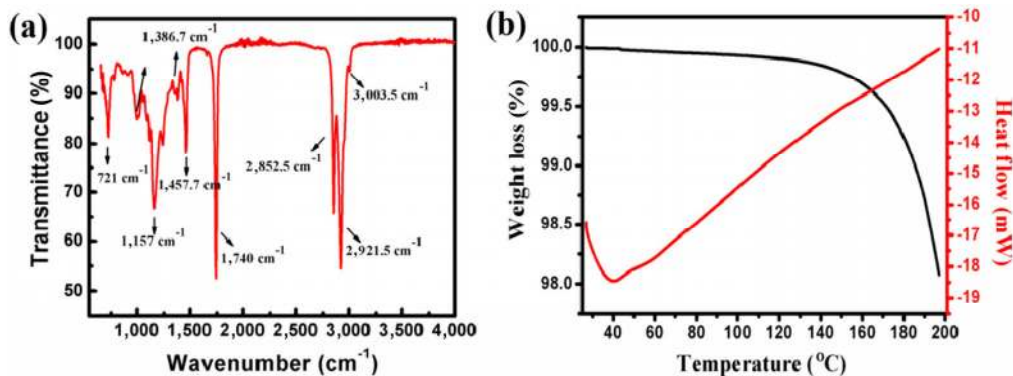


**Fig. 3** (a) IR spectrum and (b) TGA–DTA curve of vegetable oil.

in the FTIR spectra, there is a less intense but distinctly observable peak at  $3,003\text{ cm}^{-1}$ , which is due mainly to the presence of unsaturated bonds. Hence, we can confirm the presence of saturated and unsaturated bonds in the base oil.

### 3.3 Dispersion stability

The dispersion stability of  $\text{TiO}_2/\text{gC}_3\text{N}_4$  nanoadditive in the vegetable oil was investigated using UV–visible spectroscopy in the range of 350 to 650 nm. The study was performed on all of the prepared concentrations mentioned, i.e., 0.00625, 0.0125, 0.0187, and 0.0250 mg/ml. This spectroscopy technique was used to monitor the settlement of nanoadditive in the vegetable oil by observing the peak absorbance intensity [50]. Figures 4(a)–4(d) show the absorption spectra of all prepared nano-oils at settling times of 0, 24, and 48 h. It can be observed from the spectrum that the peak absorbance follows a descending order pattern as concentration decreases, which is due to the settlement of the nanoadditive in the oil with respect to time. As the settling time increases, sedimentation becomes prominent due to the formation of agglomerates. Figure 4(e) shows the peak absorption plot for all of the concentrations with settling time. It can be

seen that the decrement in the peak absorption intensity for the 0.00625 mg/ml nano-oil is very low (approximately 14%) at 24 and 48 h as compared to the same at 0 h; however, for the other samples, it is approximately 30%–40% at 24 h and 40%–60% at 48 h with respect to 0 h. Thus, it can be inferred that there is less agglomerate formation in the 0.00625 mg/ml nano-oil. With increase in concentration to 0.0125, 0.0187, and 0.025 mg/ml, the peak absorption intensity decreases rapidly with settling time, which confirms the agglomeration [51]. The peak absorption intensity of the 0.025 mg/ml nano-oil dropped significantly with a decrement of 40% at 24 h and 60% at 48 h. This nano-oil concentration shows rapid settling compared to all other concentrations, which can be explained by the clustering effect [52]. The spectra of the remaining nano-oil concentrations, i.e., 0.0125 and 0.0187 mg/ml, show an almost similar trend. Figure 4(f) shows a digital photograph of the different nano-oil samples after 48 h of settlement time. It can be seen clearly that the appearance of the nano-oils is transparent, with no settlement observed at the bottom of the vials. It must be noted that in the case of the 0.00625 mg/ml nano-oil the relative concentration of the nanoadditive dispersed in the nano-oil remains the same beyond

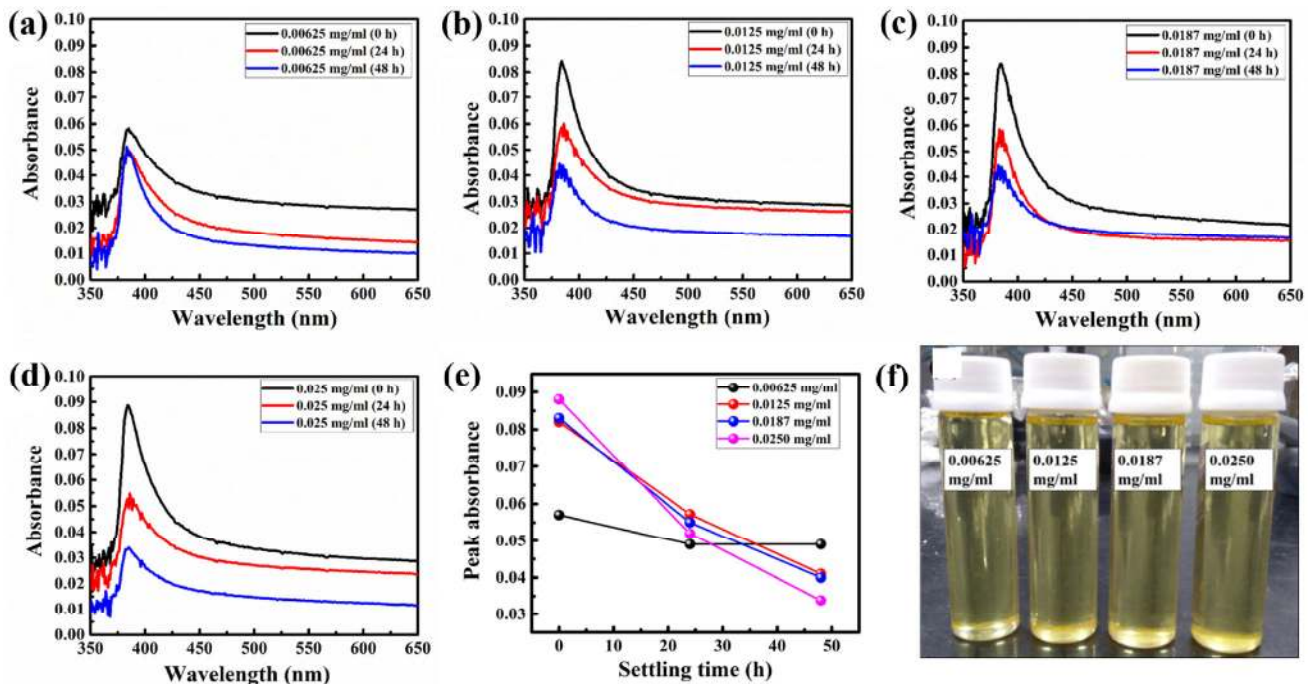


**Fig. 4** UV-visible absorption spectra of nano-oil at different concentration: (a) 0.00625 mg/ml, (b) 0.0125 mg/ml, (c) 0.0187 mg/ml, and (d) 0.025 mg/ml. (e) Relative absorbance plot for all concentrations and (f) digital photograph of the nano-oil after 48 h.

24 h. This highlights the good stability of the nano-oil at this optimized concentration. Additionally, it should be noted that this stable dispersion was obtained without the use of any surfactant. Next, to elucidate the effect of the prepared nano-oil on tribological properties, we investigated the COF for different nanoadditive concentrations.

### 3.4 Tribological behavior

Figures 5(a) and 5(b) show the change in the COF with different concentrations. The lowest COF was recorded at 0.00625 mg/ml for both operating temperatures under consideration. The COF values in the case of vegetable oil (base oil) are 0.088 and 0.09 at 29 °C and 75 °C, and the optimized nanoadditive addition

to the base oil leads to decreases in COF value of 17.0% and 23.3% at these temperatures, respectively. The important factor for evaluating the mechanism is the effective tribofilm formed on an interface, which protects the surface from damage. There are two basic parameters affecting tribofilm formation, i.e., shear and thermal effects [52]. Here, it can be seen that the COF performance of the vegetable oil becomes poorer with increase in operating temperature due to localized heating at the interface, along with a decrement in viscosity at 75 °C compared to 29 °C. Another possible reason for this result is the formation of oxidation products at 75 °C, which promotes the transition from continuous sliding to stick-slip motion. It is well reported that vegetable oil has poor stability

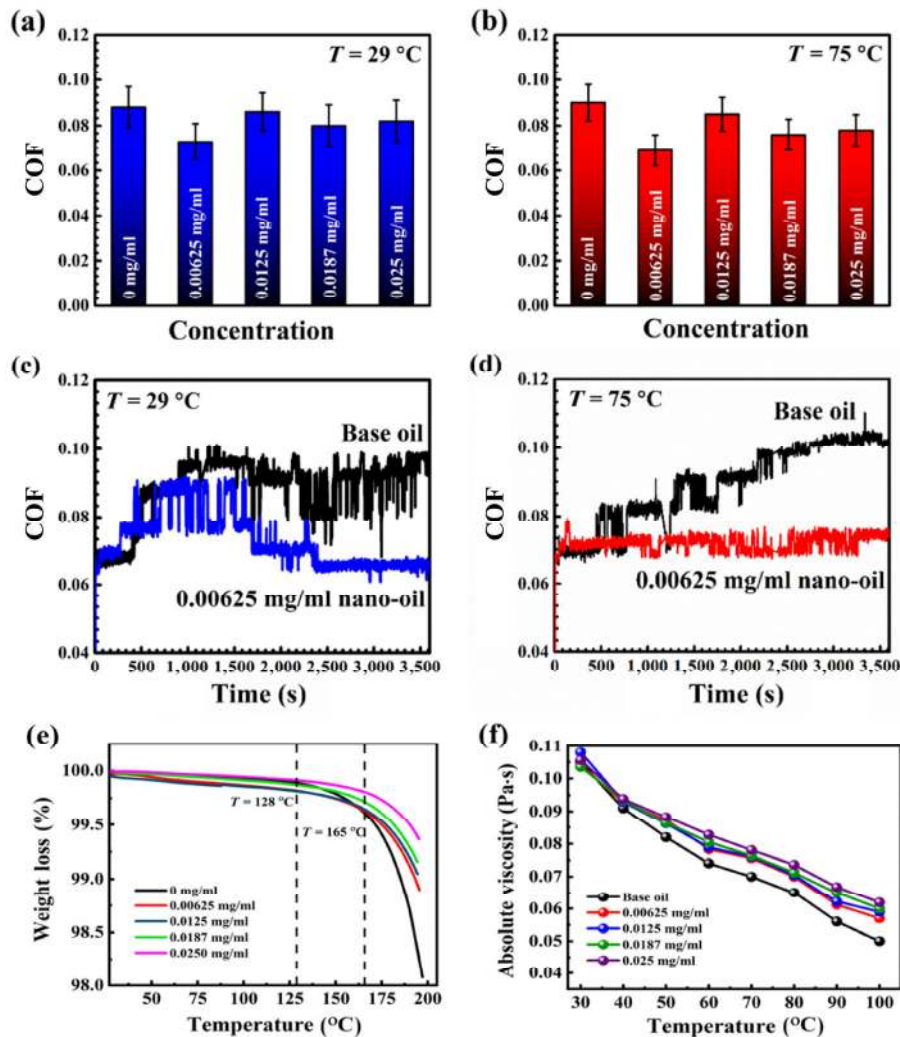


**Fig. 5** COF variation with different concentrations of nano-oil at (a) 29 °C and (b) 75 °C. COF versus time for base and 0.00625 mg/ml nano-oil at (c) 29 °C and (d) 75 °C. (e) TGA and (f) absolute viscosity plot for each nano-oil formulation.

compared to mineral oil because of the presence of unsaturated bonds, which act as active sites for many reactions, especially oxidation [33]. These unsaturated bonds lead to the formation of free radicals with the removal of hydrogen and formation of peroxy radicals, which again react with other fatty acid molecules and form hydrogen peroxide. Metals are known for being good catalysts for this reaction and hence lead to chemical and physical changes at the interface and affect lubrication performance [53]. As a result, the COF increases. The efficacy of the  $\text{TiO}_2/\text{gC}_3\text{N}_4$  addition is pronounced at higher operating temperatures because the additive controls the reaction and leads to smooth continuous sliding. To corroborate the aforementioned explanation, TGA and viscosity measurement were performed. Figure 5(e) shows the TGA curve of each oil formulation. The TGA measurement was done from RT to 200 °C, with a heating rate of 5 °C/min in an air atmosphere. The base oil TGA curve shows onset of oxidation at 128 °C, whereas the formulated nano-oil has an onset that is shifted to 165 °C. The weight loss values observed for the base oil and the nano-oil until 200 °C are 2% and 1%, respectively. The analysis leads to the conclusion that the presence of nanoadditive acts as an inhibitor that slows the rate of reaction and makes that nano-oil more thermally stable. Figure 5(f) shows the absolute viscosity plot for the base oil and nano-oil with respect to temperature. The absolute viscosity was recorded from 30 to 100 °C. The viscosities for the base oil (0.105 Pa·s) and the nano-oil (0.108 Pa·s) show similar values at 30 °C, but a significant change occurs at the higher temperature range. At 70 °C, the viscosity of the 0.00625 mg/ml nano-oil shows an 11% enhancement compared to that of the base oil. All of the formulated nano-oils show a similar trend toward the higher temperature range. It can be stated that as viscosity decreases, the COF decreases to a critical temperature; however, above the critical temperature, there is delamination of the tribofilm, leading to a continuous increase in the COF value. The delamination can occur because the Gibbs free energy increases and there is a very much lower energy requirement for the tribofilm removal as temperature increases. Here, the reason can be inferred from the continuous increase in COF of the base oil.

This observation also indicates that contact point temperature, rather than the oil temperature, plays a pivotal role for the base oil at lower operating temperatures. The presence of  $\text{TiO}_2/\text{gC}_3\text{N}_4$  in the base oil contributes to proper tribo-film formation due to the nanometer dimension of the material, which can provide a filling of asperities and maintain separation of the tribo pair. It can be seen in Figs. 5(a) and 5(b) that the maximum COF performance enhancement occurs for the 0.00625 mg/ml concentration nano-oil. Although increasing concentration of nanoadditives in the base oil may produce a better tendency for tribofilm formation, the stability of the oil should also be addressed. Further increase in nanoadditive concentration may lead to agglomeration of the nanoparticles, causing abrasive wear. To achieve the maximum reduction in COF, it is imperative to strike a balance to obtain optimum tribofilm formation together with reasonable dispersion stability and minimal agglomeration tendency. The above observations are in coherence with the UV–visible spectroscopy-based dispersion stability analysis. It may also be argued that lowering the concentration of the nano-oil further may provide better COF values. Thus, for further confirmation, the concentration of 0.00375 mg/ml was prepared and COF measurement was performed. The result obtained for the 0.00375 mg/ml concentration shows a COF curve with a similar trend as that of the base oil, with a COF value of 0.088 at 75 °C. Similar tests were also carried out with nano-oils including only  $\text{TiO}_2$  and  $\text{gC}_3\text{N}_4$  as nanoadditives for the same optimized concentration of 0.00625 mg/ml, as shown in Figs. S3(a) and S3(b) in the ESM. It was observed that the  $\text{gC}_3\text{N}_4$ -based nano-oil shows a lower COF value (0.067) until 2,000 s; after 2,000 s, a rough profile was observed. However, in the case of the  $\text{TiO}_2$ -based nano-oil, the COF value (0.073) was constant throughout the measurement. Figure S4 in the ESM shows SEM images of worn surfaces of the  $\text{TiO}_2$ -based and  $\text{gC}_3\text{N}_4$ -based nano-oils. The wear scar diameter observed was larger for the  $\text{TiO}_2$ -based nano-oil than the  $\text{gC}_3\text{N}_4$ -based nano-oil. It can be concluded from the COF and the wear scar diameter that  $\text{gC}_3\text{N}_4$  acts as a frictional modifier due to the in-plane sliding behavior, whereas  $\text{TiO}_2$  acts as an antiwear additive by filling interface asperities.

Figures 5(c) and 5(d) show the COF as a function of time for both the base oil and the optimized nano-oil. It can be observed that the friction curve for the base oil is unstable and shows increasingly higher values with increasing time for both operating temperatures. Over the duration of the experiment, which is 60 min, the COF increased from 0.07 to 0.11. This type of fluctuating and unstable friction curve is attributable to the unstable oil and intermittent seizing, breaking of the tribofilm, which leads to debris generation during the runtime in the case of vegetable oil. In contrast to the behavior of the base oil, the nano-oil exhibits a much more stable friction curve with a smooth continuous sliding motion. The presence of the  $\text{TiO}_2/\text{gC}_3\text{N}_4$  leads to proper tribofilm formation, which suppresses debris generation and consequently results in superior COF values due to polishing as well as the pushed interlayer sliding mechanism that occurs with this stable oil.

Figure 6 shows the associated mechanism at the tribo-pair interface along with the FTIR spectrum of the base oil and nano-oil (0.00625 mg/ml) used before and after the measurement. The mechanism suggests that the presence of nanoadditives provides a mending effect as  $\text{TiO}_2$  nanoparticles fill the wear debris and leads to a smoother surface in addition with the  $\text{gC}_3\text{N}_4$ . In addition to this result, IR analysis was also performed here to evaluate the oxidation behavior of the base oil before and after measurement. The earlier discussion of the IR spectrum of the base oil confirmed the presence of saturated and unsaturated bonds and the role of unsaturated bonds in oxidation. It can be seen from Fig. 6 that the IR spectra of the combined base and nano-oil before and after measurement are almost the same as those observed for the base oil shown in Fig. 3. Apart from these similar peaks, the base oil (after measurement) provides an additional peak at  $965\text{ cm}^{-1}$ , which corresponds to the increase in double bonds during thermal oxidation [54]. Additionally, there is a decrease in the peak intensity observed for  $3,003\text{ cm}^{-1}$ , which corresponds to a decrease of  $\text{C}=\text{CH}$  bonds. However, for the nano-oil, it remains the same before and after measurement. Therefore, the analysis confirms that the presence of nanoadditive inhibits the oxidation of the base oil.

To account for the other tribological properties, wear scar diameter (WSD) and wear rate calculations

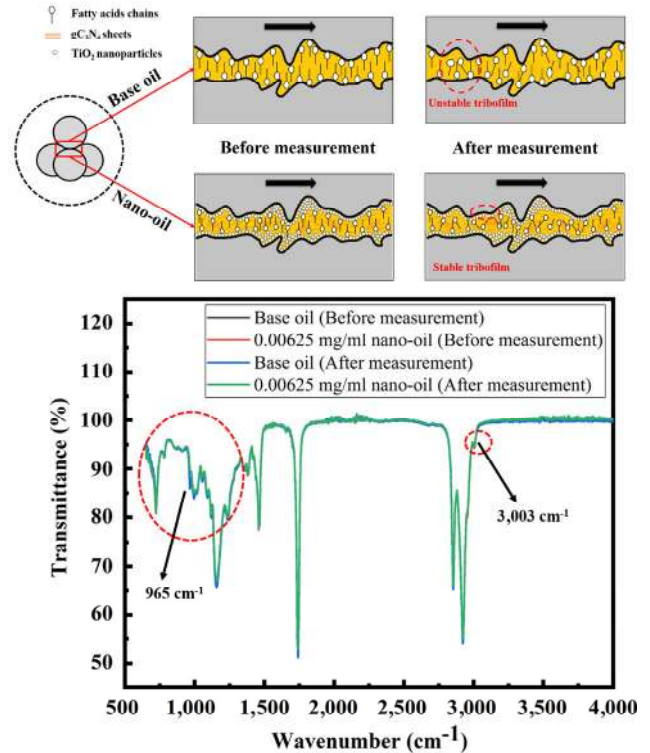


**Fig. 6** Interface mechanism of the steel tribo-pair and FTIR spectrum of base and nano-oil before and after measurement.

were also done [33]. The equations are listed in the ESM. Figures 7(a) and 7(b) show the WSD plots for different concentrations of nano-oil. The WSD values observed for vegetable oil are 0.357 and 0.492 mm at 29 and 75 °C, respectively. The indent of the observed wear scar is tear-drop shaped for the vegetable oil at 29 and 75 °C, respectively, and the nano-oil (0.00625 mg/ml) at 29 °C, as shown in Fig. 9 [55]. It is well-known from the equilateral pyramid geometry of steel balls that the force exerted by the top ball in the direction normal to the plane of contact gives circular wear scars. However, this is the case of perfect lubrication, where continuous smooth sliding occurs. Here, by examining the COF curves of vegetable oil at 29 and 75 °C and the nano-oil at 29 °C, it can be seen that the curves reflect stick-slip motion with improper tribofilm formation due to the presence of hydroxide radicals. This leads to irregular jerks, whereas the dispersion of the  $\text{TiO}_2/\text{gC}_3\text{N}_4$  in the vegetable oil leads to a decrease in WSD for all concentrations; however, the decrease is more profound in the case of 75 °C due to the already present stable oxides and nitrides, which allow the forming of a

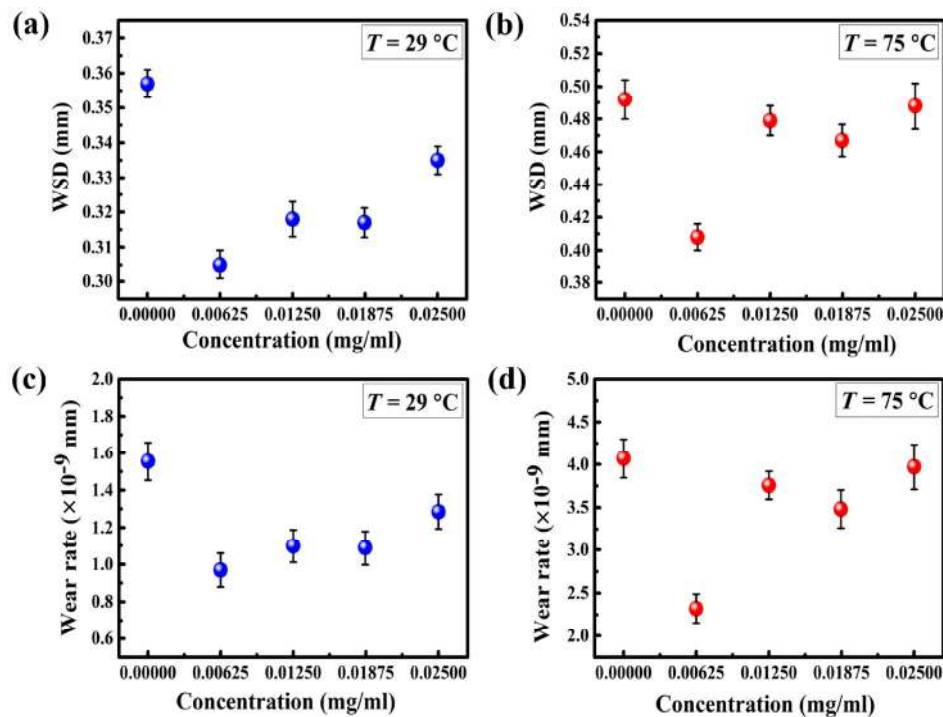


**Fig. 7** WSD plot with varying concentration of nano-oil at (a) 29 °C and (b) 75 °C. Wear rate plot with varying concentration of nano-oil at (c) 29 °C and (d) 75 °C.

stable tribofilm until the polishing and mending effects shown in Figs. 7(a) and 7(b). This is also true for the wear rate data displayed in Figs. 7(c) and 7(d). This trend in tribo-performance behavior is consistent with the COF data for vegetable oil. It can be seen that the presence of  $\text{TiO}_2/\text{gC}_3\text{N}_4$  causes a reduction in WSD, thus highlighting the improvement in the ability of the nano-oil to form a stable and adherent tribo-film that keeps the contacting steel ball surfaces separated. Maximum reductions in WSD of 14.6% and 17.1% were recorded for the 0.00625 mg/ml nano-oil at 29 and 75 °C, respectively. Similarly, wear rate reduction was found to be highest for the 0.00625 mg/ml nano-oil for both operating temperatures. It has already been pointed out that this concentration is the optimized value for  $\text{TiO}_2/\text{gC}_3\text{N}_4$ . Figure 8 shows that the presence of the nanoadditive had an influence on the rate of temperature rise of the oil during the time of the experimental runs. It can be seen that the base oil had a rapid rise in temperature for the fixed time of the experiment when compared with the nano-oils. Also, the nano-oil with the concentration of 0.00625 mg/ml had the lowest temperature rise. This observation may be interpreted in terms of lesser

intimate contact between the two steel balls due to proper tribofilm formation. Because the chance of intimate contact decreases, the temperature rise slope is shallower.

The wear scar images of the steel ball under different operating temperatures for the base and optimized nano-oil are shown in Fig. 9. Figures 9(a) and 9(e) show the wear scar of vegetable oil at low and high magnification, respectively, for the temperature of 29 °C. It can be discerned clearly that surface damage was caused by improper tribofilm formation. The

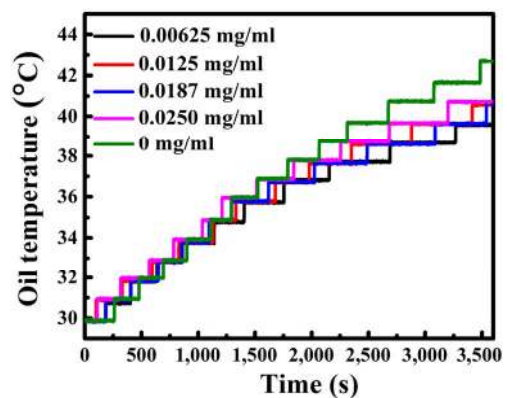


**Fig. 8** Variation in oil temperature of different nano-oil concentrations with time.

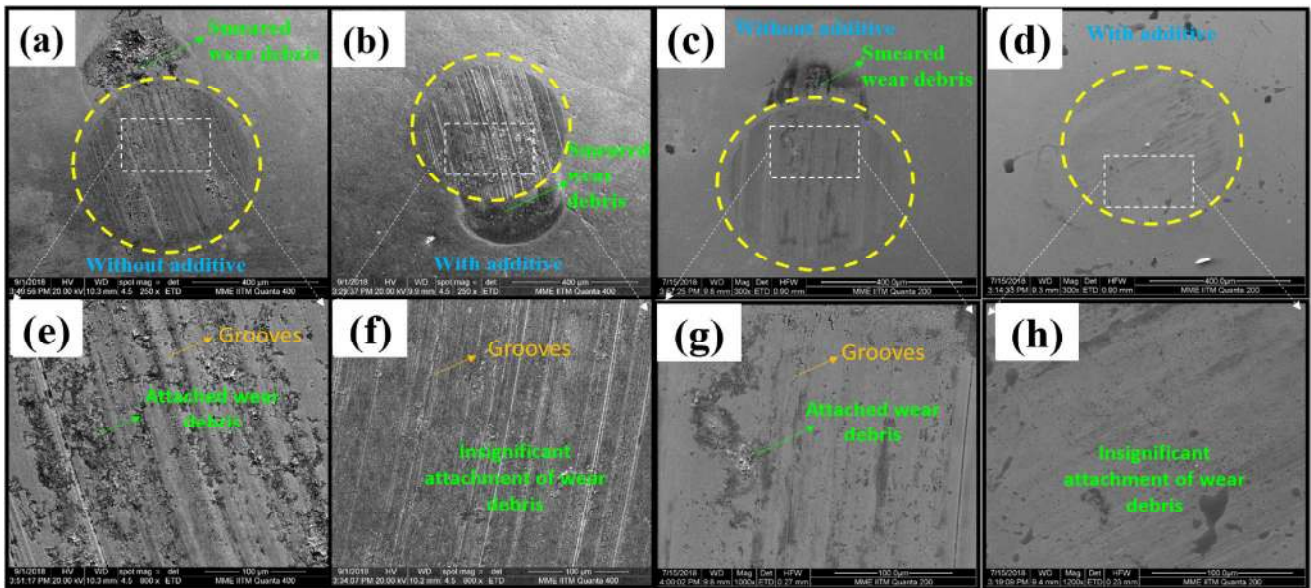


**Fig. 9** SEM micrograph of worn surfaces at 29 °C: (a, e) base oil, (b, f) 0.00625 mg/ml nano-oil, and worn surfaces at 75 °C: (c, g) base oil, (d, h) 0.00625 mg/ml nano-oil.

presence of grooves can also be observed. The formation of such damage may be attributed to the interaction of the steel ball surface with the debris generated during the runtime. Thus, there is ample indication of severe surface damage and wear in the case of vegetable oil at 29 °C. Figures 9(b) and 9(f) show the wear scar condition of the 0.00625 mg/ml nano-oil at low and high magnification, respectively, at the temperature of 29 °C. In comparison, it can be seen that the degree of damage inflicted on the surface is quite low compared to the case of the vegetable oil. Figures 9(c) and 9(g) show the wear scar of vegetable oil at low and high magnification, respectively, for the temperature of 75 °C. The wear surface shows wear debris caused by the stick-slip motion and the abrasive nature. Similarly, Figs. 9(d) and 9(e) show the wear scar condition of the 0.00625 mg/ml nano-oil at low and high magnification, respectively, at the temperature of 75 °C. The surface is relatively deficient of grooves and damage. This observation is consistent with the COF value described in the previous section. However, the tear-drop shaped scar zone had a reduced size compared to that of the vegetable oil for both of the temperatures, leading to circular scar formation at the optimized nano-oil concentration. This may be attributable to the nanoadditive introduction, which suppresses such extended damage formation by

resisting the formation and propagation of free radicals, which cause degradation of metal surfaces. This also protects the surface by forming a stable tribofilm that provides a polishing and mending effect to the surface [56]. Furthermore, these were also analyzed using surface roughness.

Optical profilometry was carried out to probe more deeply into the effect of the  $\text{TiO}_2/\text{gC}_3\text{N}_4$  on the surface and the depth profile of the wear scar zone. Figure 10 shows the surface roughness analysis for the cases of the vegetable oil and the nano-oil for both operating temperatures. Figures 10(a), 10(b), 10(e), and 10(f) show the surface roughness for vegetable oil at 29 and 75 °C, respectively. The root mean square surface roughness ( $S_q$ ) values observed for the vegetable oil are 731 and 1,078 nm at 29 and 75 °C, respectively. Surface roughness was observed more in the 75 °C case because of the unstable tribofilm formation due to the reaction of unsaturated bonds present in the vegetable oil, whereas the reaction did not occur in the case of 29 °C. Figures 10(c), 10(d), 10(g), and 10(h) show the surface roughness for the optimized nano-oil (0.00625 mg/ml) at 29 and 75 °C, respectively. It can be seen that surface roughness decreases from 731 to 524 nm as  $\text{TiO}_2/\text{gC}_3\text{N}_4$  is added to the vegetable oil at 29 °C. Similarly, when  $\text{TiO}_2/\text{gC}_3\text{N}_4$  is added to the vegetable oil at 75 °C, surface roughness decreases

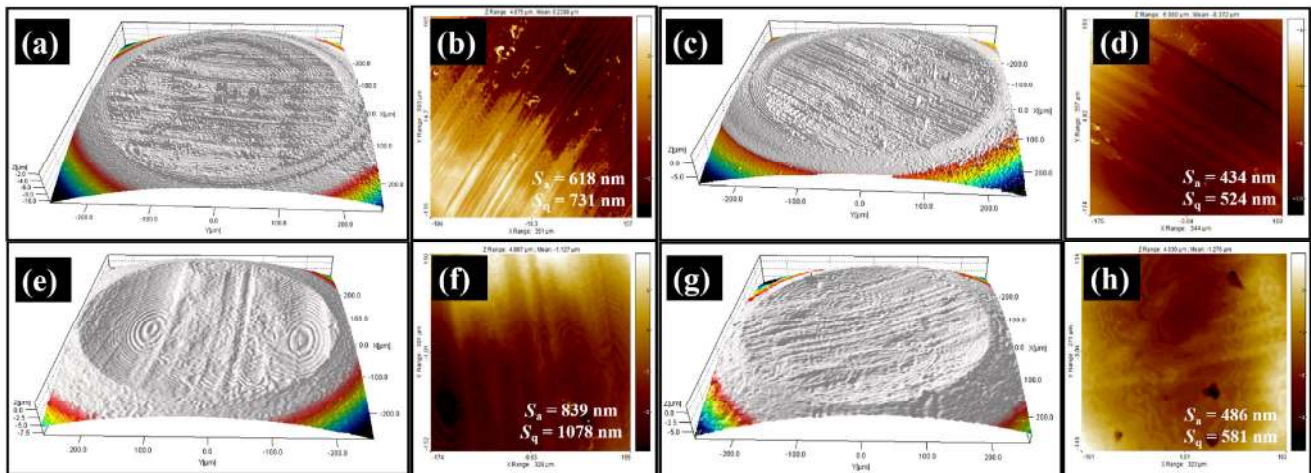


**Fig. 10** Optical profilometry images of worn surfaces along with surface roughness values: (a, b) at 29 °C and (e, f) at 75 °C for base oil, (c, d) at 29 °C and (g, h) at 75 °C for 0.00625 mg/ml nano-oil.

from 1,078 to 581 nm. The presence of  $\text{TiO}_2/\text{gC}_3\text{N}_4$  led to surface roughness decreases of 28.3% and 46.10% at the temperatures of 29 and 75 °C, respectively. The surface roughness of the wear scar region is a measure of the abrasive, adhesive, or combination wear that takes place during the course of the experiment. It may be noted that the effect of  $\text{TiO}_2/\text{gC}_3\text{N}_4$  is lower at lower temperatures. This may be attributed to the fact that the viscosity and poor tribofilm formation of the vegetable oil exhibit a dominant role in friction reduction at lower operating temperatures. However, the dispersion of the  $\text{TiO}_2/\text{gC}_3\text{N}_4$  in the vegetable oil improves the wear and tribological characteristics at room as well as elevated temperatures.

## 4 Conclusions

In this work, we showed that the use of  $\text{TiO}_2/\text{gC}_3\text{N}_4$  nanocomposite dispersed in vegetable oil can produce enhanced lubrication behavior for tribological applications. The effective decoration of  $\text{TiO}_2$  nanoparticles on  $\text{gC}_3\text{N}_4$  sheets produces the synergistic effects of the anti-wear behavior of  $\text{TiO}_2$  and the interlayer sliding behavior of  $\text{gC}_3\text{N}_4$  sheets. The as-prepared nanoadditive dispersion is very stable for the optimized nano-oil in the absence of any surfactant. The efficiency of the nanoadditive was analyzed with respect to COF, WSD, wear rate, and surface roughness. A COF reduction of 23.3% and a decline in wear scar diameter of 17.1% were recorded. Additionally, the wear rate

and surface roughness decreased by 43.0% and 46%, respectively. The optimized nano-oil with a concentration of 0.00625 mg/ml exhibits the best lubrication behavior. The proposed mechanism suggests that the presence of nitrides and oxides in the nanoadditive protect the oil from the oxidation occurring due to the unsaturated bonds with the added protection from the mending behavior. These results prove the potential viability of  $\text{TiO}_2/\text{gC}_3\text{N}_4$ -based nanolubricant for improving friction and wear resistance in the area of tribology.

## Acknowledgements

The authors thank the Department of Science and Technology (DST) for the financial support to establish Nano Functional Materials Technology Centre (NFMTC) through SR/NM/NAT/02-2005 project. Also, we would like to thank IIT Madras, Chennai, India. The SEM and Optical profilometry imaging have been carried out in Department of Metallurgical & Materials Engineering, IIT Madras.

**Electronic Supplementary Material:** Supplementary material is available in the online version of this article at <https://doi.org/10.1007/s40544-019-0336-9>.

**Open Access:** This article is licensed under a Creative Commons Attribution 4.0 International License, which permits use, sharing, adaptation, distribution and

reproduction in any medium or format, as long as you give appropriate credit to the original author(s) and the source, provide a link to the Creative Commons licence, and indicate if changes were made.

The images or other third party material in this article are included in the article's Creative Commons licence, unless indicated otherwise in a credit line to the material. If material is not included in the article's Creative Commons licence and your intended use is not permitted by statutory regulation or exceeds the permitted use, you will need to obtain permission directly from the copyright holder.

To view a copy of this licence, visit <http://creativecommons.org/licenses/by/4.0/>.

## References

- [1] Mobarak H M, Niza Mohamad E, Masjuki H H, Kalam M A, Al Mahmud K A H, Habibullah M, Ashraful A M. The prospects of biolubricants as alternatives in automotive applications. *Renew Sustain Energy Rev* **33**: 34–43 (2014)
- [2] Salimon J, Salih N, Yousif E. Biolubricants: Raw materials, chemical modifications and environmental benefits. *Eur J Lipid Sci Technol* **112**(5): 519–530 (2010)
- [3] Panchal T M, Patel A, Chauhan D D, Thomas M, Patel J V. A methodological review on bio-lubricants from vegetable oil based resources. *Renew Sustain Energy Rev* **70**: 65–70 (2017)
- [4] Bowden F P, Gregory J N, Tabor D. Lubrication of metal surfaces by fatty acids. *Nature* **156**(3952): 97–101 (1945)
- [5] McNutt J, He Q. Development of biolubricants from vegetable oils via chemical modification. *J Ind Eng Chem* **36**: 1–12 (2016)
- [6] Syahrullail S, Kamitani S, Shakirin A. Performance of vegetable oil as lubricant in extreme pressure condition. *Procedia Eng* **68**: 172–177 (2013)
- [7] Fox N J, Stachowiak G W. Vegetable oil-based lubricants—A review of oxidation. *Tribol Int* **40**(7): 1035–1046 (2007)
- [8] Gallego R, Arteaga J F, Valencia C, Díaz M J, Franco J M. Gel-like dispersions of HMDI-cross-linked lignocellulosic materials in castor oil: Toward completely renewable lubricating grease formulations. *ACS Sustainable Chem Eng* **3**(9): 2130–2141 (2015)
- [9] Colclough T. Role of additives and transition metals in lubricating oil oxidation. *Ind Eng Chem Res* **26**(9): 1888–1895 (1987)
- [10] Bongfa B, Syahrullail S, Abdul Hamid M K, Samin P M. Suitable additives for vegetable oil-based automotive shock absorber fluids: An overview. *Lubr Sci* **28**(6): 381–404 (2016)
- [11] Quinchia L A, Delgado M A, Reddyhoff T, Gallegos C, Spikes H A. Tribological studies of potential vegetable oil-based lubricants containing environmentally friendly viscosity modifiers. *Tribol Int* **69**: 110–117 (2014)
- [12] Hammes G, Mucelin K J, Da Costa Gonçalves P, Binder C, Binder R, Janssen R, Klein A N, De Mello J D B. Effect of hexagonal boron nitride and graphite on mechanical and scuffing resistance of self lubricating iron based composite. *Wear* **376–377**: 1084–1090 (2017)
- [13] Bartz W J. Solid lubricant additives—effect of concentration and other additives on anti-wear performance. *Wear* **17**(5–6): 421–432 (1971)
- [14] Kalyani, Rastogi R B, Kumar D. Synthesis, Characterization, and tribological evaluation of SDS-stabilized magnesium-doped zinc oxide ( $Zn_{0.88}Mg_{0.12}O$ ) nanoparticles as efficient antiwear lubricant additives. *ACS Sustainable Chem Eng* **4**(6): 3420–3428 (2016)
- [15] Rokosz M J, Chen A E, Lowe-Ma C K, Kucherov A V, Benson D, Paputa Peck M C, McCabe R W. Characterization of phosphorus-poisoned automotive exhaust catalysts. *Appl Catal B: Environ* **33**(3): 205–215 (2001)
- [16] Shahnazar S, Bagheri S, Abd Hamid S B. Enhancing lubricant properties by nanoparticle additives. *Int J Hydrogen Energy* **41**(4): 3153–3170 (2016)
- [17] Spear J C, Ewers B W, Batteas J D. 2D-nanomaterials for controlling friction and wear at interfaces. *Nano Today* **10**(3): 301–314 (2015)
- [18] Dai W, Kheireddin B, Gao H, Liang H. Roles of nanoparticles in oil lubrication. *Tribol Int* **102**: 88–98 (2016)
- [19] Li H, Somers A E, Rutland M W, Howlett P C, Atkin R. Combined nano- and macrotribology studies of Titania lubrication using the oil-ionic liquid mixtures. *ACS Sustainable Chem Eng* **4**(9): 5005–5012 (2016)
- [20] Zhang L, He Y, Zhu L, Yang C, Niu Q H, An C L. In situ alkylated graphene as oil dispersible additive for friction and wear reduction. *Ind Eng Chem Res* **56**(32): 9029–9034 (2017)
- [21] Ilie F, Covaliu C. Tribological properties of the lubricant containing titanium dioxide nanoparticles as an additive. *Lubricants* **4**(2): 12 (2016)
- [22] Laad M, Jatti V K S. Titanium oxide nanoparticles as additives in engine oil. *J King Saud Univ—Eng Sci* **30**(2): 116–122 (2018)
- [23] Fan X Q, Li W, Fu H M, Zhu M H, Wang L P, Cai Z B, Liu J H, Li H. Probing the function of solid nanoparticle structure under boundary lubrication. *ACS Sustainable Chem Eng* **5**(5): 4223–4233 (2017)

- [24] Chandrabhan S R, Jayan V, Parihar S S, Ramaprabhu S. Development of a nitrogen-doped 2D material for tribological applications in the boundary-lubrication regime. *Beilstein J Nanotechnol* **8**(1): 1476–1483 (2017)
- [25] Eswaraiiah V, Sankaranarayanan V, Ramaprabhu S. Graphene-based engine oil nanofluids for tribological applications. *ACS Appl Mater Interfaces* **3**(11): 4221–4227 (2011)
- [26] De Sousa J M, Botari T, Perim E, Bizao R A, Galvao D S. Mechanical and structural properties of graphene-like carbon nitride sheets. *RSC Adv* **6**(80): 76915–76921 (2016)
- [27] Cui F Z, Li D J. A review of investigations on biocompatibility of diamond-like carbon and carbon nitride films. *Surf Coat Technol* **131**(1–3): 481–487 (2000)
- [28] Zhang L G, Qi H M, Li G T, Wang D A, Wang T M, Wang Q H, Zhang G. Significantly enhanced wear resistance of PEEK by simply filling with modified graphitic carbon nitride. *Mater Des* **129**: 192–200 (2017)
- [29] Zhu L, Wang Y, Hu F, Song H J. Structural and friction characteristics of g-C<sub>3</sub>N<sub>4</sub>/PVDF composites. *Appl Surf Sci* **345**: 349–354 (2015)
- [30] Yang J, Zhang H T, Chen B B, Tang H, Li C S, Zhang Z Z. Fabrication of the g-C<sub>3</sub>N<sub>4</sub>/Cu nanocomposite and its potential for lubrication applications. *RSC Adv* **5**(79): 64254–64260 (2015)
- [31] Kumar A, Thakre G D, Arya P K, Jain A K. 2D structured Nano-sheets of octadecylamine grafted graphitic-carbon nitride (g-C<sub>3</sub>N<sub>4</sub>) as lubricant additives. *Macromol Symp* **376**(1): 1700009 (2017)
- [32] Yang G B, Zhang J F, Zhang S M, Yu L G, Zhang P Y, Zhu B L. Preparation of triazine derivatives and evaluation of their tribological properties as lubricant additives in poly-alpha olefin. *Tribol Int* **62**: 163–170 (2013)
- [33] Kumar A, Thakre G D, Arya P K, Jain A K. Influence of operating parameters on the tribological performance of oleic acid-functionalized Cu nanofluids. *Ind Eng Chem Res* **56**(13): 3527–3541 (2017)
- [34] Jaiswal V, Kalyani, Umrao S, Rastogi R B, Kumar R, Srivastava A. Synthesis, characterization, and tribological evaluation of TiO<sub>2</sub>-reinforced boron and nitrogen co-doped reduced graphene oxide based hybrid nanomaterials as efficient antiwear lubricant additives. *ACS Appl Mater Interfaces* **8**(18): 11698–11710 (2016)
- [35] Song W, Yan J N, Ji H B. Tribological study of the SOCNTs@MoS<sub>2</sub> composite as a lubricant additive: Synergistic effect. *Ind Eng Chem Res* **57**(20): 6878–6887 (2018)
- [36] Liu L, Jiao S L, Peng Y T, Zhou W. A green design for lubrication: Multifunctional system containing Fe<sub>3</sub>O<sub>4</sub>@MoS<sub>2</sub> nanohybrid. *ACS Sustainable Chem Eng* **6**(6): 7372–7379 (2018)
- [37] Ingole S, Charanpahari A, Kakade A, Umare S S, Bhatt D V, Menghani J. Tribological behavior of Nano TiO<sub>2</sub> as an additive in base oil. *Wear* **301**(1–2): 776–785 (2013)
- [38] Shakeel M, Jabeen F, Shabbir S, Asghar M S, Khan M S, Chaudhry A S. Toxicity of Nano-titanium dioxide (TiO<sub>2</sub>-NP) through various routes of exposure: A review. *Biol Trace Elem Res* **172**(1): 1–36 (2016)
- [39] Shah S N A, Shah Z, Hussain M, Khan M. Hazardous effects of titanium dioxide nanoparticles in ecosystem. *Bioinorg Chem Appl* **2017**: 4101735 (2017)
- [40] Leyva-Porras C, Toxqui-Teran A, Vega-Becerra O, Miki-Yoshida M, Rojas-Villalobos M, García-Guaderrama M, Aguilar-Martínez J A. Low-temperature synthesis and characterization of anatase TiO<sub>2</sub> nanoparticles by an acid assisted sol-gel method. *J Alloys Compd* **647**: 627–636 (2015)
- [41] Zhang Y J, Liu J, He R R, Zhang Q, Zhang X Z, Zhu J. Synthesis of aluminum nitride nanowires from carbon nanotubes. *Chem Mater* **13**(11): 3899–3905 (2001)
- [42] Zheng Y, Zhang Z S, Li C H. A comparison of graphitic carbon nitrides synthesized from different precursors through pyrolysis. *J Photochem Photobiol A: Chem* **332**: 32–44 (2017)
- [43] Rahaman O, Mortazavi B, Dianat A, Cuniberti G, Rabczuk T. A structural insight into mechanical strength of graphene-like carbon and carbon nitride networks. *Nanotechnology* **28**(5): 055707 (2017)
- [44] Zhao Z Q, Sun Y J, Dong F. Graphitic carbon nitride based nanocomposites: A review. *Nanoscale* **7**(1): 15–37 (2015)
- [45] Li F T, Zhao Y, Wang Q, Wang X J, Hao Y J, Liu R H, Zhao D S. Enhanced visible-light photocatalytic activity of active Al<sub>2</sub>O<sub>3</sub>/g-C<sub>3</sub>N<sub>4</sub> heterojunctions synthesized via surface hydroxyl modification. *J Hazard Mater* **283**: 371–381 (2015)
- [46] Vaskova H, Buckova M. Thermal degradation of vegetable oils: Spectroscopic measurement and analysis. *Procedia Eng* **100**: 630–635 (2015)
- [47] Erhan S Z, Sharma B K, Perez J M. Oxidation and low temperature stability of vegetable oil-based lubricants. *Ind Crops Prod* **24**(3): 292–299 (2006)
- [48] Alexa E, Dragomirescu A, Pop G, Jianu C, Dragoş D. The use of FT-IR spectroscopy in the identification of vegetable oils adulteration. *J Food, Agric Environ* **7**(2): 20–24 (2009)
- [49] Saad B, Wai W T, Lim B P. Comparative study on oxidative decomposition behavior of vegetable oils and its correlation with iodine value using thermogravimetric analysis. *J Oleo Sci* **57**(4): 257–261 (2008)
- [50] Mansour D E A, Atiya E. Application of UV/Vis spectroscopy to assess the stability of oil-based nanofluids. In *Proceedings of 2016 IEEE Conference on Electrical Insulation and Dielectric Phenomena*, Toronto, 2016: 671–674.

- [51] Sh M S, Fard F G, Khatibi E, Sarpoolaky H. Dispersion and stability of carbon black nanoparticles, studied by ultraviolet–visible spectroscopy. *J Taiwan Inst Chem Eng* **40**(5): 524–527 (2009)
- [52] Bhatta J I. Clusters formation during sedimentation of dilute suspensions. *Sep Sci Technol* **21**(9): 37–41 (1986)
- [53] Mannekote J K, Kailas S V. The effect of oxidation on the tribological performance of few vegetable oils. *J Mater Res Technol* **1**(2): 91–95 (2012)
- [54] Rohman A, Che Man Y B. Application of FTIR spectroscopy for monitoring the stabilities of selected vegetable oils during thermal oxidation. *Int J Food Prop* **16**(7): 1594–1603 (2013)
- [55] Brown Jr E D. Friction and wear testing with the modern four-ball apparatus. *Wear* **17**(5–6): 381–388 (1971)
- [56] Lee K, Hwang Y, Cheong S, Choi Y, Kwon L, Lee J, Kim S H. Understanding the role of nanoparticles in Nano-oil lubrication. *Tribol Lett* **35**(2): 127–131 (2009)



**Nisha RANJAN.** She received her integrated M. Tech. degree in nanotechnology in 2016 from Central University of Jharkhand, Jharkhand, India. After her master’s degree,

she joined Department of Physics, Indian Institute of Technology Madras, Chennai, India in 2016 to pursue the Ph.D. degree. Her research interest includes the synthesis of nanoparticles and its application in energy conservation and conversion systems.



**Sundara RAMAPRABHU.** He received the Ph.D. degree in physics from Indian Institute of Technology Madras, Chennai. Then, Dr. Ramaprabhu worked at Darmstadt, Germany for 2 years as an Alexander von Humboldt-Stiftung (AvH) Fellow

and for 5 years at University of Geneva, Switzerland. He joined IITM, Chennai an assistant professor and subsequently became Institute Chair Professor. He is a DAAD Fellow, Visiting Fellow to Germany by

BMBF & DFG German Science Foundations, Visiting Fellow to Republic of Korea and Japan. He is a member of American Chemical Society and member of Electrochemical Society. His research areas are nanotechnology, hydrogen energy technology, fuel cell technology, PV, Li ion battery, nanofluids, water purification, and CO<sub>2</sub> capture. He has supervised 38 Ph.D. students and developed 10 technologies. He has published articles in 370 international journals of repute and has 40 patents.